Journal of
MATERIALS RESEARCH

Oxidation and crystallization of an amorphous $Zr_{60}Al_{15}Ni_{25}$ alloy

X. Sun, S. Schneider, U. Geyer, W. L. Johnson, and M-A. Nicolet
California Institute of Technology, Pasadena, California 91125

(Received 23 January, 1995; accepted 5 June, 1996)

The amorphous ternary metallic alloy $Zr_{60}Al_{15}Ni_{25}$ was oxidized in dry oxygen in the temperature range 310 °C to 410 °C. Rutherford backscattering (RBS) and cross-sectional transmission electron microscopy (TEM) studies suggest that during this treatment an amorphous layer of zirconium-aluminum-oxide is formed at the surface. Nickel was depleted in the oxide and enriched in the amorphous alloy near the interface. The oxide layer thickness grows parabolically with annealing duration, with a transport constant of 2.8×10^{-5} $m^2/s \times \exp(-1.7\ eV/kT)$. The oxidation rate may be controlled by the diffusion of Ni in the amorphous alloy. At later stages of the oxidation process, precipitates of nanocrystalline ZrO_2 appear in the oxide near the interface. Finally, two intermetallic phases nucleate and grow simultaneously in the alloy, one at the interface and one within the alloy. An explanation involving preferential oxidation is proposed.

I. INTRODUCTION

Recently, a novel group of amorphous metallic alloys such as ZrAlNi,[1] ZrAlCu,[2] ZrAlNiCu,[3] and ZrTiNiCuBe[4] with excellent glass-forming ability and high thermal stability has been discovered. Most of these alloys are Zr-based, and highly reactive with oxygen. It is therefore of general interest and practical relevance to study the mechanism of oxidation and its influence on nucleation of crystalline phases near the glass transition temperature. The present study examines the temperature-dependent oxidation behavior of the amorphous $Zr_{60}Al_{15}Ni_{25}$ alloy.

II. EXPERIMENTAL

$Zr_{60}Al_{15}Ni_{25}$ ingots were prepared by induction melting on a water-cooled copper boat under a Ti-gettered argon atmosphere. Small pieces of the initial ingot were levitation-melted in a high-frequency rf field. The samples were subsequently quenched into thin foils in a pure argon-filled twin-piston rapid quencher. The thickness of these quenched foils is about 50 μm.

The foils were exposed to dry oxygen in an open-ended quartz-tube furnace over a temperature range of 310 °C to 410 °C. The oxygen gas flow was adjusted to 100 cm^3/min. Other samples were annealed in a vacuum-tube furnace with a base pressure of 4×10^{-7} Torr.

Rutherford backscattering spectrometry (RBS) was performed to analyze the concentration depth profiles using 2.0 MeV and 6.2 MeV $^4He^{2+}$ ions. RBS data analysis was performed using the standard procedures.[5] In order to study the structure of the as-quenched and annealed foils, x-ray diffraction using Co K_α radiation ($\lambda = 0.1790$ nm) was applied. The microstructure and composition of the samples were also studied by TEM and analyzed by energy-dispersive analysis of x-rays (EDS). These samples were prepared by a microtome technique.

III. RESULTS

A. Oxide composition and growth kinetics from 310 °C to 410 °C

Figure 1 shows the backscattering spectra of $Zr_{60}Al_{15}Ni_{25}$ foils, as-quenched and annealed at 370 °C for various duration. The signal of the light element Al is barely resolved over the background of the Zr and Ni yields. Spectra of the annealed samples reveal that the Zr is oxidized at the surface, as the reduced height

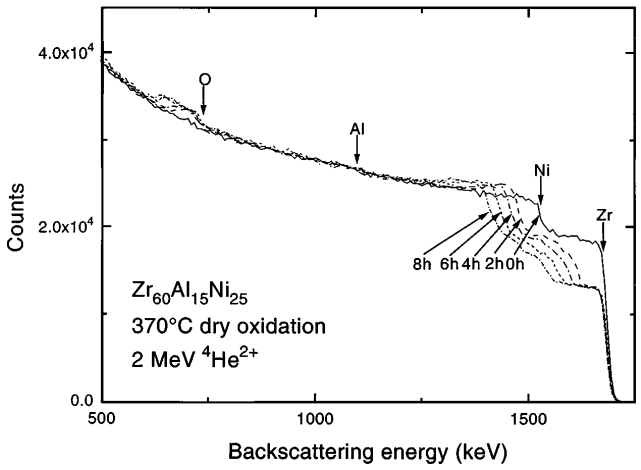

FIG. 1. Backscattering spectra of $Zr_{60}Al_{15}Ni_{25}$ amorphous foils before and after annealing in dry oxygen at 370 °C for various duration. (The incident beam is normal to sample surface; scattering angle of detected particles is 170°.) The levels marked on the right abscissa are explained in the text.

of its high energy signal proves. In addition, an oxygen plateau appears at the low-energy end of the spectra. The Ni signal moves to lower energies, indicating that Ni is expelled from the growing oxide layer. We conclude that during annealing a homogeneous surface oxide layer grows. The height of the surface near Zr signal is consistent with the oxide composition of $Zr_8Al_2O_{19}$,[5] where the Zr : Al atomic ratio is the same as in the nonoxidized alloy, and Zr and Al have the same valence as in their most common oxides ZrO_2 and Al_2O_3. The Ni signal also rises above its prior height on the low energy side of the Ni step. This excess signal broadens with annealing duration, but its maximum height stays constant, which implies that the Ni concentration near the interface increases to a fixed value. For further investigations, the oxide thickness was calculated from the energy shift of the high-energy Ni edge.

Backscattering spectra (not shown) of the samples oxidized between 310 °C and 410 °C depict similar depth profiles as described above for 370 °C. The Ni concentration in the alloy just below the interface is independent of the annealing temperature and about 35 at. %. X-ray diffractometry and TEM studies show that the underlying alloy and the oxide layer formed remained amorphous in all samples up to the longest annealing duration investigated here (see Fig. 4 for a sample annealed 8 h at 370 °C).

Figure 2 shows for several temperatures a linear relation between the square of the oxide thickness and the annealing duration. Least-squares fits are also presented. To convert the shift of the Ni edge in the backscattering spectra to the oxide thickness, the atomic density of amorphous Zr–Al–O is required. Since no data are available, this density was estimated by a linear combination of amorphous ZrO_2[6] and crystalline Al_2O_3[7] according to the 4 : 1 Zr to Al cation ratio, which results in an atomic density for the amorphous Zr–Al–O phase of 6.9×10^{22} cm^{-3}. The transport constants were derived from the slope of the least-square fits.

The logarithms of these constants as a function of the reciprocal temperature are shown in Fig. 3. The data can be fitted by a straight line

$$\ln \frac{K}{K_0} = -\frac{E_a}{kT},$$

where the value of K_0 is found to be $2.8(3) \times 10^{-5}$ m^2/s, and the activation energy E_a is 1.70(5) eV/atom (164 kJ/mol).

Since both the Zr and Al are uniformly distributed throughout the oxide, it is possible that oxygen is the dominant moving species in this reaction, and that the oxidation takes place at the oxide/alloy interface. The other less likely case is that Zr and Al migrate through the oxide at rates that will maintain an unchanged Zr to Al atomic ratio upon their oxidation at the surface.

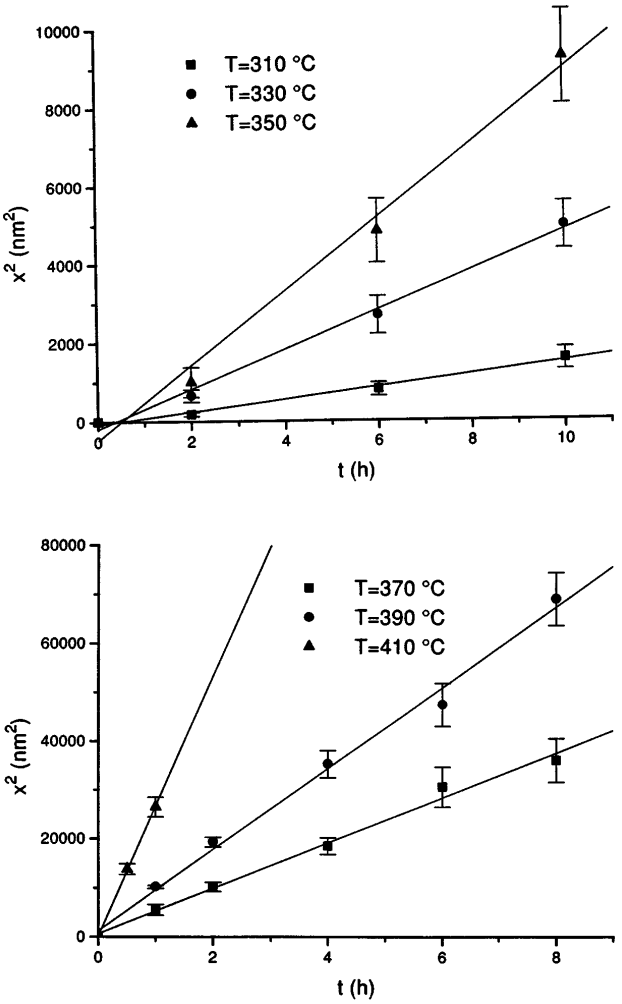

FIG. 2. The square of the oxide thickness, x, versus oxidation duration at temperatures from 310 °C to 410 °C.

Most likely, the scenario for the oxidation process at 370 °C is the following: oxygen is transported through the oxide layer to the interface, where it reacts with Zr and Al, while Ni diffuses back into the amorphous alloy. The experimentally observed parabolic growth of the oxide layer indicates that the oxide growth is not controlled by a possible interfacial reaction, but transport limited. According to this interpretation of the backscattering spectrometry results, two diffusion processes are involved: the diffusion of oxygen in the oxide, and of nickel in the alloy. However, the steady-state Ni enrichment at the interface suggests that Ni diffusion through the alloy may be the rate-determining process.

B. Oxidation and crystallization at 410 °C

The backscattering spectra of samples oxidized at 410 °C for various duration (not shown) are similar to

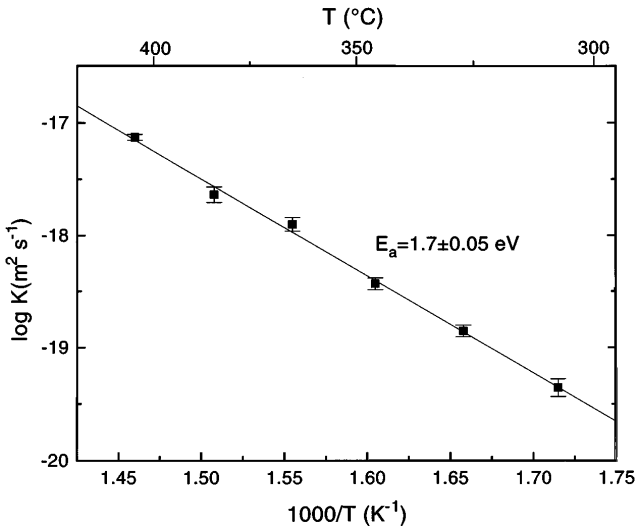

FIG. 3. Arrhenius plot of the transport constant from 310 °C to 410 °C.

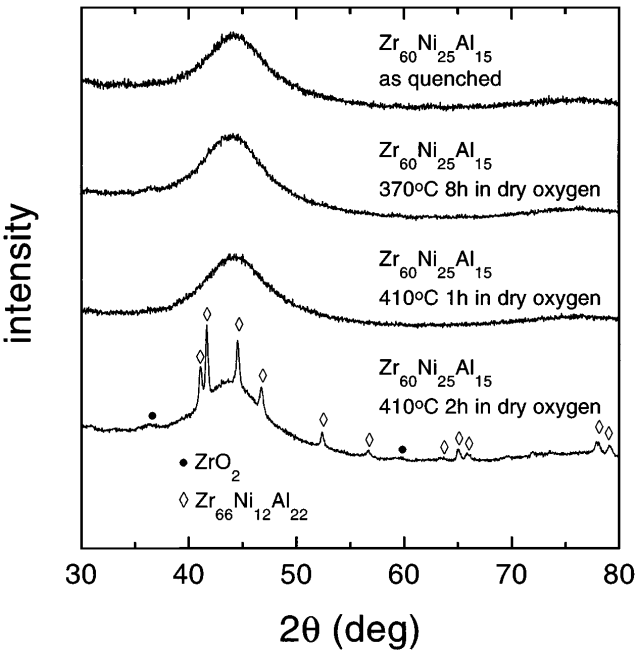

FIG. 4. X-ray diffraction spectra of foils before and after annealing in dry oxygen at 370 °C for 8 h and at 410 °C for 1 h and 2 h (Co K_α, $\lambda = 0.17902$ nm).

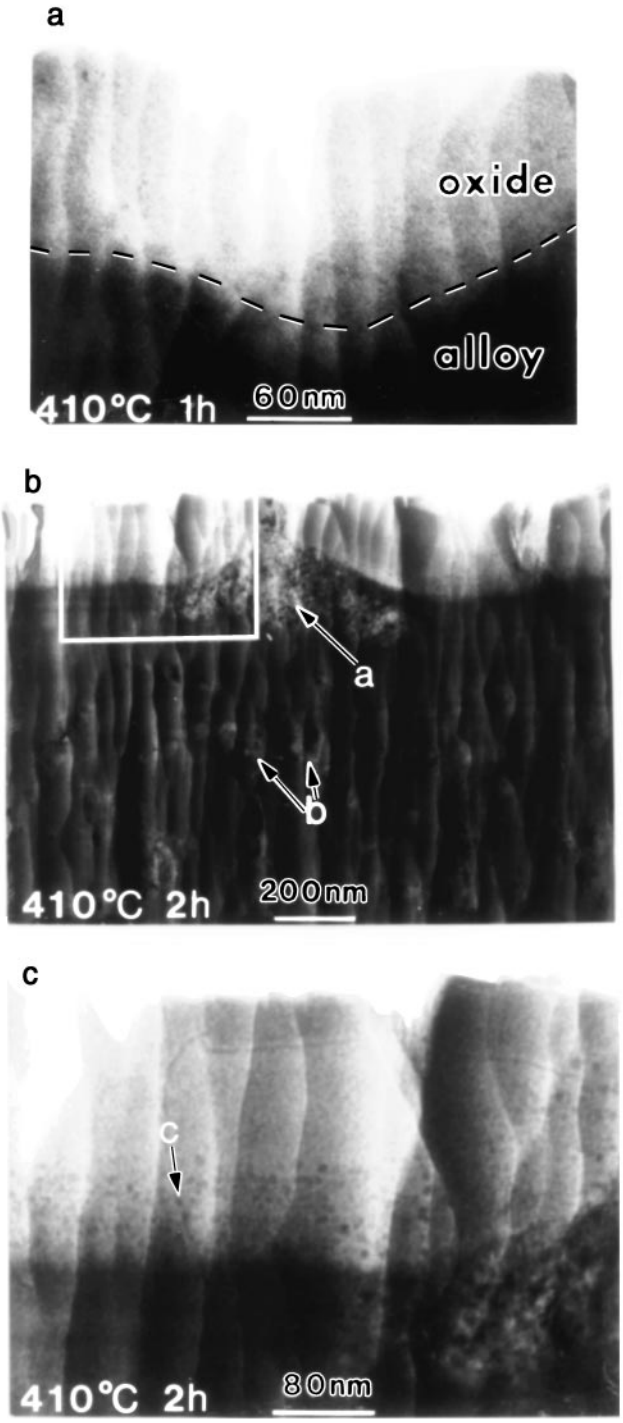

FIG. 5. Bright-field transmission electron micrographs of foils after annealing at 410 °C in dry oxygen for 1 h (a) and 2 h (b). Figure (c) shows the framed area in (b). Arrows used in (b) and (c) point to (a) a cluster of Zr_5Ni_4Al nanograins at the interface, (b) nanocrystalline Zr_6NiAl_2 phase inside the alloy, and (c) nanocrystalline ZrO_2 particles embedded in the amorphous oxide near the interface.

those of Fig. 1 for oxidation at 370 °C and reveal the same layered structure and its evolution with time.

X-ray diffraction spectra of an as-quenched foil and of one annealed for 1 h at 410 °C depict only the broad signal of an amorphous structure (Fig. 4). A bright-field transmission electron micrograph [Fig. 5(a)] shows that an oxide layer has formed after 1 h of annealing. The horizontal scratches (direction of microtoming) and the band-shaped vertical structure of the cross-sectional micrographs are typical of microtomed samples.[8]

The depth distribution of the metal elements in the oxide and beyond was obtained by EDS from a cross-sectional sample of a foil annealed for 1 h at 410 °C (Fig. 6). The diagram shows the relative intensities of the Ni K_α, Zr K_α, and Al K_α signals as a function of depth. The interface, defined as the point at half-maximum Ni concentration, is indicated in the diagram. The measured intensities do not change beyond 200 nm from the surface where the corresponding concentration is $Zr_{60}Al_{15}Ni_{25}$. It is not possible to derive the atomic compositions of the elements in the oxide from these data because oxygen cannot be detected by EDS in our setup using a Be window. In agreement with backscattering spectrometry, the Ni content within the experimental error is zero in the surface layer, and increases rapidly near the interface, reaching a maximum at 150 nm in depth. The transition region has a thickness of about 60 nm. The thickness of the surface oxide layer is about 120 nm.

An x-ray spectrum for foils oxidized for 2 h reveals Bragg peaks (Fig. 4) of a cubic ZrO_2 phase and of the intermetallic compound Zr_6NiAl_2.[9] An estimate based on the Debye–Scherrer formula indicates that the average grain size of these oxide particles is only a few nanometers.

The transmission electron micrographs of this sample [Figs. 5(b) and 5(c)] reveal many nanocrystals embedded in the amorphous oxide layer near the interface (arrow c). These nanocrystals were too small for unambiguous EDS or electron diffraction analysis, but they probably correspond to the ZrO_2 phase depicted in the x-ray spectrum. A cluster of grains is observed across the interface in the middle of the micrograph B (arrow a). EDS analysis exhibits that this cluster contains a Ni-rich phase ZrNiAl phase, which is not detected by x-ray diffraction because of its small volume fraction. Crystalline particles of the Zr_6NiAl_2 phase are embedded in the matrix of the amorphous alloy (arrow b).

C. Oxidation of $Zr_{72.5}Al_{15}Ni_{12.5}$ at 330 °C

In this final section, we show that a minor variation in alloy composition changes the results significantly. We have oxidized an alloy with half as much Ni (12.5 instead of 25 at. %) and correspondingly more Zr (72.5% instead of 60%). These samples still preserve an amorphous structure after quenching and subsequent oxidation at 330 °C. Figure 7 shows two RBS spectra of amorphous $Zr_{60}Al_{15}Ni_{25}$ and amorphous $Zr_{72.5}Al_{15}Ni_{12.5}$, both oxidized at 330 °C for 2 h, together with that of the as-quenched foil of $Zr_{72.5}Al_{15}Ni_{12.5}$. The energy of the $^4He^{2+}$ beam was 6.2 MeV to take advantage of the enhanced scattering cross section of oxygen in the 6.0 to 6.2 MeV range.[10] The enhanced oxygen signal indicates that both annealed samples form a planar oxide layer with about the same thickness, but additionally, oxygen is detected beyond the oxide/alloy interface in the Ni-lean sample (see inset in Fig. 7). From this spectrum, we estimate that the oxygen content in this sample drops monotonically behind the oxide layer from about 25 at. % at the interface to 0 at. % some 70 nm inside the alloy.[5]

This result implies an elevated content of oxygen in the Ni-lean alloy. The oxygen just below the interface might exist as a solid solution of oxygen in the

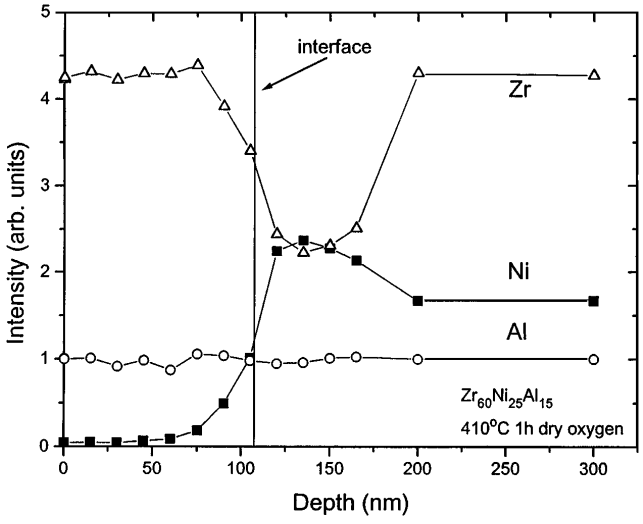

FIG. 6. Relative intensities of the Ni K_α, Zr K_α, and Al K_α signals from energy-dispersive analysis of x-rays as a function of depth for a sample annealed in dry oxygen at 410 °C for 1 h.

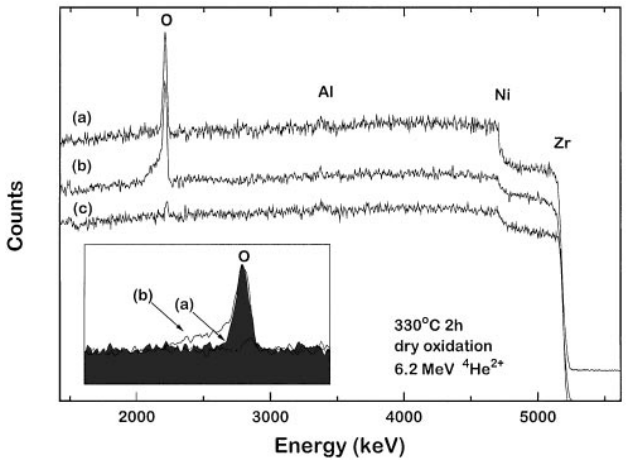

FIG. 7. 6.2 MeV $^4He^{2+}$ backscattering spectra (incident beam normal to sample surface, scattering angle of detected particles is 177°) of amorphous foils $Zr_{60}Al_{15}Ni_{25}$ (a), and $Zr_{72.5}Al_{15}Ni_{12.5}$ (b), both annealed at 330 °C for 2 h in dry oxygen. For comparison, a spectrum of the as-prepared $Zr_{72.5}Al_{15}Ni_{12.5}$ sample is plotted in (c). The spectra are shifted vertically for clarity. The inset shows an enlarged portion of the unshifted spectra near the oxygen signal.

amorphous alloy. An alternative view is that in the case of the Ni-rich alloy, oxygen cannot penetrate into the alloy below the oxide because the accumulated Ni at the interface blocks the in-diffusion of oxygen. This again implies that oxygen is the faster diffuser. On the other hand, the diffusion rate of Ni may not differ in both alloys, since both oxide layers have the same thickness.

IV. DISCUSSION

Birchenall, in a review paper,[11] discussed oxidation in the case of an alloy that contains both a relatively active element and a more noble one. Here, preferential oxidation of the active element may take place, and the back-diffusion of the noble element can become rate-controlling, provided that its mobility is lower than that of the oxidant in the oxide, and also that the alloy does not dissolve an appreciable amount of oxygen.

The oxidation process of the polycrystalline Ge_xSi_{1-x} system has recently been described in detail.[12] This binary system behaves in a generally similar fashion to the ternary $Zr_{60}Al_{15}Ni_{25}$ system. Silicon dioxide is thermodynamically more stable than GeO_2.[13] However, at low temperatures, the motion of Ge and Si is essentially frozen and the oxidant reacts with both Ge and Si as it reaches the interface by diffusion. As the temperature increases, the system transitions gradually from uniform to preferential oxidation. At the transition temperature, the Ge–Si–O formed has an increasingly higher Si to Ge ratio than the alloy. When the transition is complete, Ge is fully rejected from the oxide and accumulates behind the oxide interface. In the amorphous alloy $Zr_{60}Al_{15}Ni_{25}$, Zr is the most reactive and Ni the most noble element with respect to oxidation, based on a comparison of the free energy of formation of the corresponding stable oxides at low temperatures.[13] Nickel is also expected to be the most mobile among the three elements in the alloy due to its small atomic size compared to Zr and Al. Since the $Zr_{60}Al_{15}Ni_{25}$ is a ternary system, two transition temperatures might exist. The first one could be below 310 °C, where all three elements are oxidized simultaneously. Above the first transition temperature, Ni becomes more mobile and is gradually excluded. This has been described above.

A preferential oxidation of Zr over Al is not observed at temperatures below 410 °C. In this temperature range, the Al and Zr atoms are kinetically frozen and the chemical equilibration of the oxides with the metal phases is suppressed. At about 410 °C, Al, the second smallest atom of the alloy, becomes more mobile, and after 1 h the nanocrystalline ZrO_2 starts to form at the interface. Isolated particles of preferential oxide have also been observed earlier in oxidized Fe–Ni alloys.[14] An explanation for the mechanism is given by Wagner.[15]

This second transition takes place at 410 °C, when Al begins to be rejected from the oxide during oxidation. The transition starts locally, but its detailed progression cannot be traced further as the crystallization starts at the interface after 2 h of oxidation.

At the same time when the ZrO_2 nanocrystals form, the entire amorphous alloy starts to crystallize. To examine the relation between the crystallization of the amorphous matrix and the formation of the ZrO_2 nanocrystals, an unoxidized foil was annealed in vacuum at 410 °C for 2 h. Transmission electron micrographs of this foil (not shown) reveal grains embedded in the amorphous matrix of the alloy, like in the sample annealed in oxygen ambient. The size of the grains is about the same as those observed in the alloy side of the oxidized samples. The position of the peaks in the x-ray diffraction spectra of these two foils is exactly the same except for the presence or absence of three ZrO_2 peaks. These grains of the Zr_6NiAl_2 phase are formed inside the alloy of samples annealed in both vacuum and oxygen atmosphere. Therefore, the crystallization of the amorphous $Zr_{60}Al_{15}Ni_{25}$ alloy at 410 °C seems to be independent of the oxidation and probably has the same reason as the formation of crystalline ZrO_2 in the oxidized samples: the increasing mobility of Al at $T \geqslant 410$ °C.

V. SUMMARY

Preferential oxidation is observed at the surface of amorphous $Zr_{60}Al_{15}Ni_{25}$ alloy foils. Zr and Al are uniformly oxidized at a temperature range 310 °C to 390 °C with the Zr/Al ratio in the oxide similar to that in the alloy. The foils and the oxide remain fully amorphous. We suggest that the growth of the oxide may be controlled by the Ni back-diffusion in the alloy. At 410 °C, the intermetallic compound Zr_6NiAl_2 appears in the alloy, and a Ni-rich ZrNiAl phase nucleates near the alloy/oxide interface.

This study supports literature reports that in some alloys which contain a relatively reactive element and a relatively noble one, a transition temperature exists from uniform to the preferential oxidation. The oxidation is homogeneous below this temperature. As temperature rises, the mobility of the noble element increases, and it is rejected from the alloy at the interface. The growth of the oxide layer is controlled by the diffusion of the rejected noble element.

The onset of crystallization of the amorphous alloy takes place at 410 °C. X-ray diffraction and transmission electron microscopy reveal that this crystallization is independent of the oxidation.

ACKNOWLEDGMENTS

We gratefully acknowledge Professor T. Tombrello for providing access to the tandem accelerator for the

6.2 MeV $^4He^{2+}$ backscattering spectrometry. We thank C. Garland for technical help on the transmission electron microscopy. Financial support for this work was provided by the United States Department of Energy (No. DEFG-03-86ER45242) and by the Army Research Office. Technical assistance by R. Gorris, M. Easterbrook, and A. Rice is also acknowledged.

REFERENCES

1. A. Inoue, T. Zhang, and T. Masumoto, Mater. Trans. JIM **31**, 177 (1990).
2. A. Inoue, T. Zhang, and T. Masumoto, Mater. Sci. Eng. **A178**, 255 (1994).
3. T. Zhang, A. Inoue, and T. Masumoto, Mater. Trans. JIM **32**, 1005 (1991).
4. A. Peker and W. L. Johnson, Appl. Phys. Lett. **63**, 2342 (1993).
5. W. K. Chu, J. W. Mayer, and M-A. Nicolet, *Backscattering Spectrometry* (Academic Press, New York, 1978).
6. K. Sugiyama, Y. Waseda, and S. Kudo, ISIJ Int. **31**, 1362 (1991).
7. *CRC Handbook of Chemistry and Physics,* edited by R. C. Weast and M. J. Astle (CRC Press, Inc., West Palm Beach, FL, 1979), p. B92.
8. D. H. Kay, *Techniques for Electron Microscopy,* 2nd ed. (F. A. Davis, Philadelphia, 1965), Chap. 8.
9. O. Kubaschewski, C. B. Alcock, and P. J. Spencer, *Materials Thermochemistry,* 6th ed. (Pergamon Press, Oxford, 1993).
10. Z. Zhuying, in *High Energy and Heavy Ion Beams in Materials Analysis,* edited by J. R. Tesmer, C. J. Maggiore, M. Nastasi, J. C. Barbour, and J. W. Mayer (Mater. Res. Soc. Symp. Proc. **HIB**, Pittsburgh, PA, 1990).
11. C. E. Birchenall, *Oxidation of Alloys* (American Society for Metals, Metals Park, OH, 1970), Chap. 13.
12. S-G. Park, W. S. Liu, and M-A. Nicolet, J. Appl. Phys. **75**, 1764 (1994).
13. I. Barin, *Thermochemical Data for Pure Substances* (VCH Verlagsgesellschaft mbH, D-6940 Weinheim, Germany, 1989).
14. K. Sachs, J. Iron Steel Inst. **187**, 93 (1957).
15. C. Wagner, J. Electrochem. Soc. **103**, 571 (1956).